



THE UNIVERSITY *of* EDINBURGH

Edinburgh Research Explorer

Optical access schemes for high speed and spatial resolution optical absorption tomography in energy engineering

Citation for published version:

Tsekenis, S & Polydorides, N 2017, 'Optical access schemes for high speed and spatial resolution optical absorption tomography in energy engineering', *IEEE Sensors Journal*.
<https://doi.org/10.1109/JSEN.2017.2715364>

Digital Object Identifier (DOI):

[10.1109/JSEN.2017.2715364](https://doi.org/10.1109/JSEN.2017.2715364)

Link:

[Link to publication record in Edinburgh Research Explorer](#)

Document Version:

Peer reviewed version

Published In:

IEEE Sensors Journal

General rights

Copyright for the publications made accessible via the Edinburgh Research Explorer is retained by the author(s) and / or other copyright owners and it is a condition of accessing these publications that users recognise and abide by the legal requirements associated with these rights.

Take down policy

The University of Edinburgh has made every reasonable effort to ensure that Edinburgh Research Explorer content complies with UK legislation. If you believe that the public display of this file breaches copyright please contact openaccess@ed.ac.uk providing details, and we will remove access to the work immediately and investigate your claim.



Optical access schemes for high speed and spatial resolution optical absorption tomography in energy engineering

Stylianios-Alexios Tsekenis and Nick Polydorides

Abstract — Optical diagnostic techniques play an important role in the engineering of modern energy processes. Optical absorption tomography as a diagnostic technique allows imaging of chemical species in flows with spatio-temporal resolution. The optical access scheme employed to acquire the tomographic projections impacts the limiting spatial resolution and imaging speed of the instrument. Our review of conventional optical access schemes indicates that there currently exist no practical schemes that can achieve simultaneous high speed, high spatial resolution imaging. Here we show that advanced solid-state beam deflectors can be used to realize such a system. We evaluated a state of the art electro-optic deflector combining a multi-pass scheme in a space-charged crystal and found that it can achieve a full deflection angle of 216 mrad (12.4 °) at 90 kHz scan rate. We present how optical access schemes based on electro-optic deflectors can be arranged, estimating the increased bandwidth requirement for the data acquisition system. Using an existing tomography system and image reconstruction algorithm, we show by simulation that the spatial resolution under non-optimum conditions can be improved by 38%. We describe in detail our implementation of the spatial resolution quantification algorithm. Our results demonstrate how advances in other disciplines can be exploited to further improve the performance of an optical tomography instrument. We anticipate our assay to motivate further development of optical access schemes as well as optimized image reconstruction algorithms.

Index Terms—absorption tomography, chemical species, electro-optic deflectors, spatial resolution

I. INTRODUCTION

Optical absorption tomography has emerged as an important diagnostic technique to study the evolution of targeted chemical species in reactive fluid flows with temporal and spatial resolution. The technique has found numerous applications in energy research, enabling the characterization of chemical processes in combustors, automotive, marine and aviation engines. Optical absorption tomography utilizes resonant spectroscopic absorption from the target species, typically in the Near-IR or Mid-IR spectral regions, as the tomographic modality. Here we give a description of the basic principle of operation and forward model of this modality to prepare the ground for our discussion on optical access schemes and spatial resolution.

A pencil-beam traverses a non-uniform chemical species distribution at a molar concentration χ as shown in Fig. 1. The concentration varies along the beam propagation vector \mathbf{r} at a parametric location u over a pathlength U . The frequency ν of the transmitted light is selected so that the beam experiences resonant spectroscopic absorption due to the specific rotational

and vibrational energy level transitions of the species of interest. The molar concentration is governed by the Beer-Lambert law:

$$\frac{I_r}{I_t} = e^{-SP\varphi_\nu \int_0^U \chi[\mathbf{r}(u)]du} \quad (1)$$

where I_r and I_t are the intensities of the received light and transmitted light respectively, S is the line strength of the transition, P is the total pressure and φ_ν is the frequency-dependent lineshape due to broadening [1]. The temperature and pressure are assumed to be uniform. Using (1) the species concentration can be quantified as a path-concentration integral (PCI). Tomography as an extension to (1) allows quantification in two dimensions and produces synthetic cross-sectional images of the concentration distribution.

To achieve spatial resolution, a number of sampling beams, each yielding a PCI, are arranged as in Fig. 1 to traverse a Cartesian imaging space containing the species concentration distribution. The i -th beam is at a distance s_i perpendicular to the origin and forms an angle θ_i with the y -axis. A set of parallel beams is termed a tomographic projection. The concentration of the i -th beam can be written as a Fredholm integral equation of the First Kind [2]:

$$\chi_i(s_i, \theta_i) = \int_0^\infty \chi_i[\mathbf{r}(s_i, \theta_i)(u)]du \quad (2)$$

Deconvolution of (2) for realistic, low PCI-count systems is an ill-posed and ill-conditioned problem having no unique and stable solution. To make image reconstruction tractable, prior assumptions such as positivity, spatial constraints, smoothness and computational fluid dynamics models are commonly incorporated in the image reconstruction algorithm. These assumptions reduce reconstruction ambiguity at the expense of measurement objectivity. Nevertheless, for a finite number of sampling beams some ambiguity will persist, limiting the system's ability to image closely-spaced or small features as quantified by the system's limiting spatial resolution figure.

In order to improve the spatial resolution achieved by a given system, a higher density of unique PCIs is required in linear and angular dimensions. Space limitations around the imaging process compounded with the finite size of launch/receive optical components place an upper limit on the number of achievable PCIs. Consequently in practical implementations

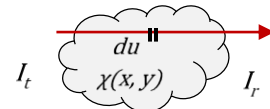


Fig. 1. A single beam experiences resonant spectroscopic absorption while traversing the imaging space containing a distribution of chemical species.

the objective is to maximize the number of sampling beams while optimizing their position and orientation in the imaging space. The optical access strategy is intrinsic to these efforts, therefore it must be carefully considered and selected.

II. REVIEW OF OPTICAL ACCESS SCHEMES IN ABSORPTION TOMOGRAPHY

In order to acquire a number of PCIs two requirements must be met: a) the process and its boundaries must be, or made optically accessible at the relevant spectral region(s) and b) a strategy to introduce a number of beams must be put in place to acquire a plurality of PCIs with spatial resolution. We proceed to review the latter, categorizing the works based on the general optical access scheme. Within each category the works are grouped based on application context and then in chronological order. Special cases are discussed last. We limited the scope to works that perform tomographic imaging based on light beam(s) having a well-defined beam-width that traverse the process of interest experiencing path-integrated resonant spectroscopic absorption. The beam(s) can either be stationary over time or scan the process. In this review we have included fan-beams due to their relevance.

A. Fixed optics and process

Systems in this category are characterized by having optical access components, sampling beams and imaging space boundaries that are permanently fixed in space. Such systems typically employ all-fiber optic light distribution combined with collimating launch and receive lenses.

Several systems have been developed to image the concentration distribution of hydrocarbon fuel inside the cylinder of an operating reciprocating engine. The imaging space is circular and optically accessible through an annular window. The systems share a similar architecture which has been conceptualized in [3]. The concept was implemented in a 32-beam system having 4 projections [4]. In one case optical access was achieved by substituting a slice of the engine block with a plate carrying fiber optics near the cylinder walls and onto ball-lens collimators forming an irregular 27-beam array [5]. The same instrumentation system was configured with a 32-beam regular array of 4 projections [6]. Tight packing of collimation optics was achieved by relying on deterministic positioning of the optics in precision-machine grooves. All works reviewed so far have dealt with spark-ignition (SI) engines. However, a compression-ignition (CI) engine has also been instrumented using an adapted version of the system described in [5]. Reference [7] reports on imaging the fuel concentration distribution inside an operating CI engine at high speed. Optical access was achieved using an annular window (similar to [4]) surrounded by launch and receive optics mounted in precision-machined grooves (similar to [6]). The installed beam array comprised 31 beams in 4 regular projections.

The in-cylinder imaging technology was extended to image methane in marine engines [8]. Two beam array designs were proposed: a 26-beam regular array to image the entire cylinder cross-section and a 31-beam irregular array to specifically target the exit orifices of the engine's pre-chamber. Miniature

optical windows allowed operation at full cylinder pressure.

In flame diagnostics, fixed-optics systems have targeted water vapor, methane or ammonia. In all cases the distribution of temperature and concentration was imaged. Reference [9] describes a hyperspectral optical absorption tomography using a total of 6 beams regularly arranged in a square imaging space. Similarly in [10], 24 beams formed a regular array in a circular imaging space. In [11] a 16-beam system with 3 projections was used to image methane in a free-space flow, ammonia in an emulated engine exhaust and methane in an oscillating circular flame.

Fixed-optic optical access has also been applied for jet engine diagnostics. Systems typically maintain significant clearance distance from the exhaust plume. The hyperspectral system of [9] was extended to utilize a total of 30 beams in 2 projections [12]. The extended system was used to image the temperature and concentration distributions of water vapor across the exhaust of a commercial turbojet engine. Full-scale imaging of carbon dioxide has recently been achieved at the exhaust of a civil aviation turbofan engine [13]. Optical access is by 126 beams arranged in 6 projections and mounted on a 7 m diameter ring surrounding the approximately 1.4 m diameter exhaust plume.

As a special case in this category, [14] reports on the measurement of temperature and pressure in a supersonic combustor. The system used 16 stationary and quasi-parallel sampling beams placed along the axial direction of the flow and traversing it span-wise. Two diagonal beams were also used to determine the flow velocity. Due to the flow pressure and temperature parameters being quasi-uniform in the span-wise direction, this scheme provided adequate spatial resolution using a single tomographic projection.

B. Translated beam or symmetric process

Systems in this category utilize a single, manually translated sampling beam to acquire multiple PCIs. In the majority of cases the process imaged is radially symmetric from a macroscopic perspective and an 'onion-peeling' algorithm [15] is used. Also included here are systems imaging asymmetric processes where implementing only a single beam greatly reduces experimental complexity.

In the case of a radially symmetric process such as a flame, in [16] the temperature of a sooting flame was measured using a light source of low temporal coherence. The flame was linearly translated to acquire 15 PCIs. Species concentration and temperature distributions in flat flames have also been imaged, targeting carbon monoxide [17] and carbon dioxide [18]. In both cases the flame was translated and 20 PCIs acquired. Optical absorption tomography has been applied in other symmetric processes. Reference [19] reports on imaging of the concentration distribution of methane on 3 axial planes in a fuel-air jet. For each plane the flame was translated to acquire 12 projections each having 87 parallel PCIs on average. Reference [20] describes imaging of the temperature and atomic number density distributions in a vacuum arc-jet motor. Measurements were taken on 3 planes using a single beam translated linearly on each plane. The number of PCIs acquired

varied as a function of the exhaust plume diameter.

Several asymmetric processes have been instrumented in different application contexts. Reference [21] describes a system to image the concentration distribution of oxygen in a rectangular flow. The system acquires a total of 486 PCIs from 6 projections by combining translation of the sampling beam and the flow. Reference [22] reports on tomographic monitoring of carbon monoxide emissions from a volcano. An open-path gas analyzer was used in combination with a retroreflector placed across the emissions plume (≈ 100 m). A total of 15 PCIs were captured with the gas analyzer rotated in two positions. Carbon monoxide was also imaged in a flat flame [23] and, similarly to the oxygen imaging application in [21], 285 PCIs were acquired by angular and linear translation of the flame. Unlike previous references here the flame was not assumed to be symmetric. Finally, reference [24] reports on imaging of hydrocarbon fuel in a model of a gas turbine combustor. The sampling beam was translated in 6 projections of 25 parallel beams each yielding 150 PCIs.

As special cases in this category, the water vapor concentration distribution in a flame was imaged in microgravity artificially created by freefall of the entire apparatus [25]. To simplify the experiment a total of 8 PCIs were acquired simultaneously using a fixed array of 8 parallel beams. Water vapor concentration was also imaged, along with temperature, in a flat flame [26]. Instead of a single translated beam, the authors used a fixed array of 12 equally spaced and parallel beams spanning the entire diameter of the flame. One half of the beam array was offset by half the beam pitch thereby doubling the spatial sampling frequency (recall that the process is radially symmetric process).

C. Continuous fan-beam illumination

Systems in this category utilize optics that form a fan-beam traversing the process being imaged. Here we use the term ‘fan-beam’ in its broader sense to describe a beam of light having a beam-width in one traverse direction that is much wider than another direction. Consequently this category also encompasses parallel sheet illumination. The fan-beam is continuous i.e. its cross-section is characterized by a continuous intensity profile and stationary. The desired number of PCIs is formed by collecting the fan-beam on a number of detectors, typically discrete photodiodes or integrated arrays of abutted photodiodes.

Fan-beam illumination has been applied in diverse applications. The density of chlorine in a supersonic flow was imaged using parallel sheet illumination and a 1024-element photodiode array [27]. The optical access setup was rotated around the flow at 6 projections with 30° angular separation thus acquiring 6144 PCIs. A general stationary fan-beam system for imaging reactive flows was described in [28]. The conceptual system uses multiple fan-beam sources placed around the process. Discrete detectors are illuminated by multiple sources that are time-division multiplexed to produce unique PCIs. To concept was demonstrated by imaging a flow of diacetyl vapor using a single fan-beam source and 96 photodetectors. The flow was rotated with respect to the fan-

beam thereby emulating a large number of projections. Two applications in laboratory flames have been reported, imaging the temperature and concentration distribution of combustion species. Reference [29] imaged a pulsed flame using 4 stationary and parallel sheets located at regular angular intervals around the flame. Each sheet was focused on a 35-element photodiode array yielding a total of 140 PCIs. Similarly, [26] imaged a flat flame using 5 fan-beams. Each beam illuminated 12 discrete photodiode detectors yielding 60 PCIs in total. Regarding packed beds, [30] reports on the measurement of water vapor at the output of a packed-bed absorber column. Three stationary parallel sheets originating from one side of the imaging space were focused on 128-element photodiode arrays yielding a total of 384 PCIs. Lastly, [31] reports on imaging of carbon monoxide as a combustion by-product. The system utilized discrete collimated fiber optics and photodiodes in a way similar to [4], [32] previously described. However, in this system the process is illuminated by 3 stationary fan-beam sources yielding 48 PCIs in total.

D. Scanning beam with stationary source

Systems in this category utilize one or more light launch sources capable of creating a scanning pencil beam. Contrary to the continuous fan-beam case, a unique line of sight measurement is conducted at any given time. The launch optics might contain moving parts to scan the beam but they remain stationary with respect to the process.

Reference [33] describes a concept scanning beam tomography system to monitor atmospheric pollutants over large geographical areas. A scanning mirror at the centre of the imaging space directs the sampling beam onto reflectors placed on the circumference of the virtual imaging space. Incident light on each reflector creates a virtual, continuous fan-beam source that illuminates a number of detectors also placed on the periphery of the process. A different system described in [34] used a similar mirror arrangement as in [33], however the beam was directed onto a screen coated with a Lambertian scatterer forming virtual cone beam sources. Scattered light from each source was collected by a subset of 90 discrete detectors equally spaced along the circumference of the imaging space. The concentration distribution and temperature of gaseous ammonia has also been demonstrated using the system described in [35]. The system utilized 4 platforms on which the launch and receive optoelectronics were mounted. The platforms rotated about themselves forming 4 scanning beams. Having traversed the imaging space, each beam was reflected by a cylindrical mirror back to the rotating platform where a photodetector was placed near the launch optics. In total 400 PCIs were acquired.

As a special case in this category, the mixture fraction of a radially symmetric flame was imaged in microgravity [36]. Similarly to the systems in section I-B, a single scanning beam source was collimated by an off-axis parabolic mirror creating a linearly-scanned beam through the flame. The beam was collected by another off-axis parabolic mirror onto a photodetector. A total of 31 PCIs were acquired to characterize the axisymmetric flame process.

E. Scanning beam and translated source

Systems in this category employ a scanning beam source that moves with respect to the imaging space during the experiment. The translation path is typically circular and the overall system geometry resembles that of a medical X-ray CT scanner.

The measurement of water vapor concentration and temperature distribution was demonstrated in a supersonic combustion tunnel [37]. Optical access was achieved by a single unit combining launch and receive elements. Inside the unit a beam of controlled divergence was launched through an aperture in an off-axis receiving mirror. Having traversed the process once, the beam was back-reflected towards the source by a cylindrical mirror. The diameter of the returning beam was larger than the aperture in the receiving mirror and so a portion of the returning beam was reflected onto a photodetector. The entire unit was mounted on a small rotary table to create a scanning beam. Subsequently, the rotary table was mounted on an annular rotary stage which positioned the rotary table 360° around the process. Both rotating mechanisms were under computer control and a total 1800 PCIs were acquired. The same system was extended by the authors to utilize five scanning beam sources and it was applied to image species concentration and temperature distribution at the exhaust of a scramjet combustor [38]. The additional sources were used to reduce acquisition time rather than increase the number of PCIs. The extended system acquired 840 PCIs in a full scan by rotating the scanning beam sources by 75°.

We identified two special cases in this category. Reference [39] developed a concept optical absorption tomography system for applications in two-phase flows. In this system the flow is sampled using, in essence, a 28-beam array formed with stationary optics and rotating at 1500 RPM. The number of PCIs is then limited by the angular positioning resolution. To our knowledge the concept has not been implemented. Reference [40] reports on a scanning beam system that is unique in the sense that it is capable of forming any beam array geometry in the imaging space. The system was applied to image water vapor concentration and temperature distribution in vapor deposition reactors. Two optical access platforms were mounted on a circular rail enclosing the process. On the first platform a light source in combination with a scanning mirror formed a single beam in the imaging space. On the second platform a second scanning mirror directed the incoming beam onto a photodetector. The position of the platforms and angle of the mirrors were electronically controlled to maintain line of sight between source and detector as the platforms were translated on the rail. This arrangement provides the necessary degrees of freedom to form a sampling beam at an arbitrary radial distance from the centre of the imaging space and angle. Therefore the entire Radon space can be sampled subject to positioning resolution and experimental time.

F. Scheme comparison and scope of paper

The performance of optical access schemes can be compared based on a wide range of metrics. Two metrics are of immediate interest for high speed, high spatial resolution tomography: a) the number of unique PCIs that can be acquired and b) the total

time required to do so. The motivation for metric (a) was described in section I, relating the number of PCIs to the limiting spatial resolution. Metric (b) stems from the requirement to image fast fluid flows in real time (<10% change between tomographic frames), typically in combustion research applications.

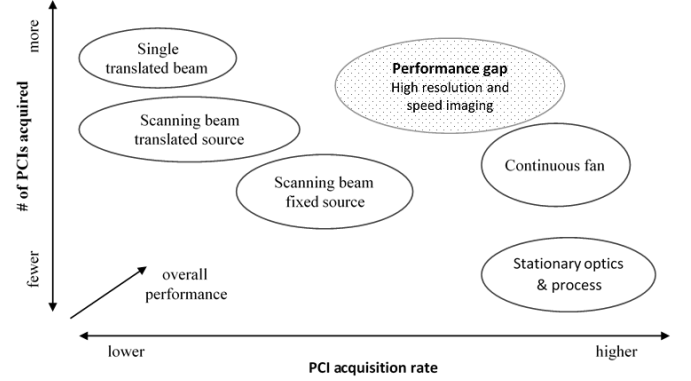


Fig. 2. Relative performance of optical access schemes reviewed in this paper.

The relative performance of the optical access schemes reviewed in this paper has been qualitatively mapped in terms of the aforementioned metrics and is shown in Fig. 2. On the right-hand side, schemes having the optics and process stationary are capable of the fastest acquisition speed due to the potential for fully parallel acquisition. Continuous-fan systems are a variation of stationary optics, thus the acquisition speed is comparable. However, in many continuous-fan systems an integrated photodiode array with serial data readout is utilised which introduces a time penalty. In both schemes, the number of PCIs that can be acquired is limited due to mechanical constraints around the process. On the left-hand side, systems with many moving parts must overcome inertia and are therefore relatively the slowest. Systems using a single translated beam offer the most flexibility in orienting the beam with respect to the process and are therefore capable of the highest number of PCIs.

Optical access schemes that can acquire a large number of PCIs at a speed in par with stationary optics remain underdeveloped. Closer to achieving the desired performance are systems utilizing fixed sources that generate either a continuous or a scanning fan beam. Comparing the two, the continuous fan scheme is easier to implement and can achieve a higher acquisition rate. However, optical power is wasted at the inter-detector space. In the case of discrete detectors where the active detector area is significantly smaller than the detector pitch, the radiant power requirement from the light source can become unrealistic. On the other hand scanning-beam systems require the equivalent radiant power of a single pencil beam at the expense of a lower acquisition rate. Scanning-beam systems can randomly access the imaging space. This is an important advantage in process engineering as the scanning pattern can be limited only to regions of interest thus avoiding optically thick or highly scattering regions in the process.

This paper aims to motivate the development of new, high performance optical access schemes enabled by recent breakthroughs in the field of solid-state beam deflectors. We

briefly review beam deflection technologies focusing on electro-optic deflectors, present fundamental optical access strategies and quantify by simulation the anticipated gain in spatial resolution performance for such novel systems.

III. BEAM DEFLECTION TECHNOLOGIES FOR TOMOGRAPHY

There exist a number of disparate beam deflection technologies to create a scanning beam [41]. The performance of each technology is presented in Fig. 3. Of particular interest are inertia-free acousto-optical deflectors (AODs) and electro-optical deflectors (EODs) as they exhibit the highest scan speed without suffering from wear, mechanical noise and drift. Moreover, EODs and AODs offer random-access scanning. Comparing AODs with EODs, the random-access response of AODs is slower due to the velocity of the acoustic wave on the crystal. More importantly, the beam deflection angle of AODs depends on the wavelength of the input beam [42] which precludes use of AODs in wavelength-scanning schemes such as Tunable Diode Laser Absorption Spectroscopy (TDLAS). Therefore our discussion is focused on EODs.

The basic principle of operation of EODs has been covered in textbooks [43], [44]. Briefly, a plane-polarized beam traversing a transparent, birefringent material is refracted due to a change in the material's refractive index when an electric field is applied (parallel to the polarization plane of the beam) across the material using electrodes. The effect is particularly pronounced in Potassium Tantalate Niobate (KTN) crystals where the change of refractive index exhibits a quadratic relationship to the applied electric field (Kerr effect) and maximum at $\approx 35^\circ\text{C}$ [45]. An additional mechanism that adds to the utility of KTN in EODs is the space-charge effect whereby electrons from the electrodes are injected in the crystal creating

where V is the applied voltage, ϵ_0 and ϵ_r is the permittivity of vacuum and KTN respectively, n is the refractive index of KTN ($V=0$), d is the thickness of the crystal, L is the interaction length of the beam in the crystal. The crystal thickness is kept small to overcome difficulties in crystal growth and electron injection. An undesirable side effect is that the clear optical aperture of the crystal also becomes small which implies a large beam divergence and susceptibility to optical aberrations. A limit exists where the angular deflection for a given voltage is overwhelmed by beam divergence. At the limit, the number of resolvable spots N is [48]:

$$N = \frac{2\theta_e w_0}{\lambda} \quad (4)$$

where w_0 is the beam waist radius and λ the wavelength. Typically, 20 to 30 resolvable spots can be achieved [49] from one source; a performance comparable to the total number of PCIs from all projections in several optical absorption tomography systems reviewed.

In order to increase the number of resolvable spots for a given aperture the interaction length must be increased. This has been the subject of recent advancement in KTN EOD technology, whereby high reflectivity coatings on the edges of the crystal made the beam traverse the crystal three times (Fig. 4a). The result was that the deflection angle and number of resolvable spots were tripled to ~ 61 [49], which represents a 300-600% increase in the number of PCIs per projection for most systems reviewed here having stationary or fan-beam optical access.

Integrated devices employing the three-pass KTN scheme, corrective optics and temperature control have been developed (NTT-AT, Japan) and are commercially available (AMS Technologies, Germany) as single or dual axis EODs.

In our laboratory we independently evaluated the single-axis version optimized for visible wavelengths (Fig. 4b). The EOD was powered by a resonant voltage amplifier controlled via LabVIEW and connected to a 635 nm laser (Thorlabs LPS-PM635-FC) via a polarization-maintaining fiber. The KTN crystal temperature was maintained at 35.4°C . An amplified photodetector with 10 MHz bandwidth (Thorlabs PDA36A) was used to measure the scan frequency. The deflection angle was measured by placing a screen at a known distance and recording the length of the scan trace (Fig. 4c). When driven with $200\text{ V}_{\text{pk-pk}}$ the setup achieved a deflection angle ($2\theta_e$) of 216 mrad at 90 kHz.

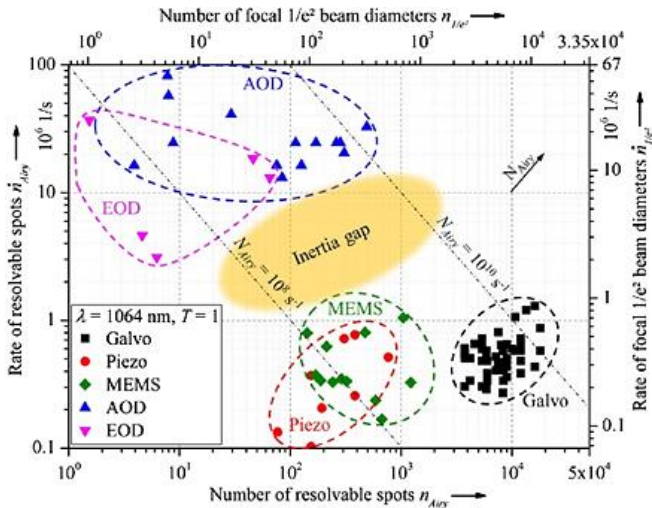


Fig. 3. Number of resolvable spots (equivalent to number of uncorrelated PCIs) versus rate of resolvable spots (equivalent to acquisition speed) for different beam deflection technologies. Adapted from [41].

an electric field gradient which causes a cumulative refraction of the beam through the crystal [46]. The combined effects cause a beam deflection angle θ_e given by [47]:

$$\theta_e = -0.153n^3\epsilon_0^2\epsilon_r^2\frac{V^2}{d^3}L \quad (3)$$

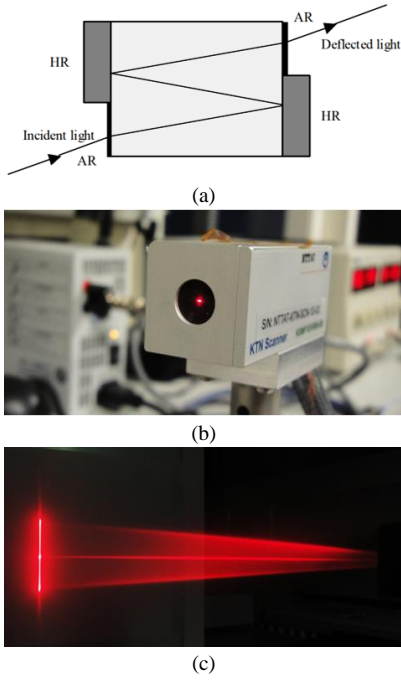


Fig. 4. (a) The deflection angle is tripled by folding the beam inside the KTN crystal by coating the sides either with an anti-reflective (AR) or a high-reflectivity (HR) film. (b) Integrated and commercially available single-axis deflector evaluated in our laboratory and (c), output scanning beam. Light of residual polarization is not deflected and appears as a static beam in the centre.

IV. OPTICAL ACCESS USING SCANNING BEAMS

Optical access for a system utilizing scanning sampling beams can be implemented using different strategies. Here we present two strategies suitable for small ($<7\text{cm}$) and large diameter imaging spaces. Additional implementations can be conceived (e.g. using retroreflectors) by the creative reader. In the case of a small diameter imaging space in Fig. 5, an optical element such as a lens can direct the attenuated sampling beam onto a single photodetector. The detected intensity is then a continuous function of the beam position and the gas parameters in its path. In the case of large imaging spaces, sourcing or fabrication of focusing optics becomes challenging.

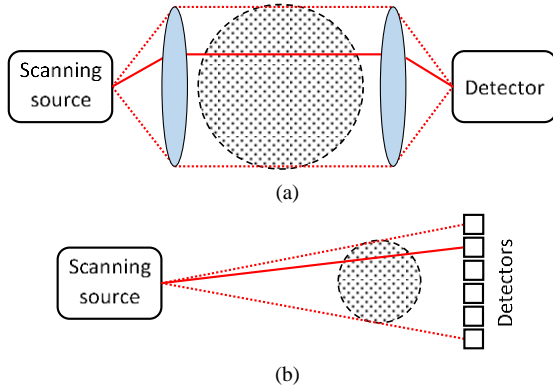


Fig. 5. Two proposed optical access strategies based on a fast scanning beam. In (a) the imaging space is small and each beam path can be acquired using a single detector. In (b) the large imaging space necessitates distinct detectors. Several variations of these strategies are possible.

In such cases discrete detectors can be used without further beam translation optics. In any case the source must be placed

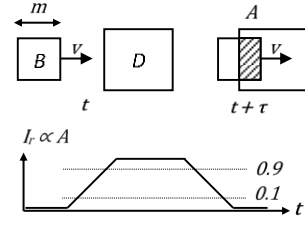


Fig. 6. A beam spot is scanned over an active detection area. The time-dependent overlap amplitude-modulates the received intensity signal.

at sufficient distance to scan the entire region of interest.

In the case where the beam is scanned over multiple discrete detectors, an additional intensity modulation component (separate to any source modulation scheme) is imposed on the signal. Here we briefly examine the bandwidth requirements imposed on the detector and subsequent instrumentation.

In Fig. 6, we assume an ideal rectangular detector 'D' and a rectangular beam spot profile 'B' of width m and having uniform irradiance. Assuming a linear detector response, the measured light intensity I_r will be proportional to the overlap area A . If the beam spot moves with constant velocity v , the detector output waveform will resemble an isosceles trapezoid with finite rise time t_r and fall time t_f given by:

$$t_r = t_f = t(0.9I_r) - t(0.1I_r) = \frac{m}{v} 0.8I_r \quad (5)$$

The velocity of the beam spot is given by:

$$v = lf \quad (6)$$

where l is the length of the scan trace on the detector plane and f is the scan frequency. If the transient response of the detection system is assumed to be that of an RC network, then the -3 dB bandwidth of the system BW is approximated as follows:

$$BW \cong \frac{0.35}{t_r} \quad (7)$$

Combining (5), (6) and (7), the bandwidth requirement for the detection system BW_d with I_r normalized to 1 is given by:

$$BW_d > \frac{0.4375lf}{m} \quad (8)$$

Letting $m = 0.5 \text{ mm}$, $l = 100 \text{ mm}$ and $BW_d = 17 \text{ MHz}$ for a commercial photodiode detector (Thorlabs PDA10CS), the maximum scan frequency $f = 194 \text{ kHz}$.

V. SPATIAL RESOLUTION OF SCANNING BEAM SYSTEM

Having shown that existing beam deflector technology can triple the number of sampling beams and thereby PCIs, we proceed to quantify the effect of the increased number of PCIs in the spatial resolution of the system.

We based our analysis on an existing optical absorption tomography system developed to image CO_2 in the exhaust plume of an aviation engine [13]. The existing system utilises a 126-beam array arranged in 6 projections each of 21 parallel beams (Fig. 7). Our objective then was to reconstruct a simulated test concentration, a 40 cm diameter sharp-edge phantom having a uniform 6% concentration, using the 126-beam array and a new, high density 378-beam array.

Increasing the number of projections was not straightforward

due to the architecture of the image reconstruction algorithm [50] which was optimised for the existing 126-beam array. Instead, we tripled the number of beams per projection from 21 to 63 and maintained the overall dimensions of the beam array. Under this non-ideal condition, artefacts arising from the

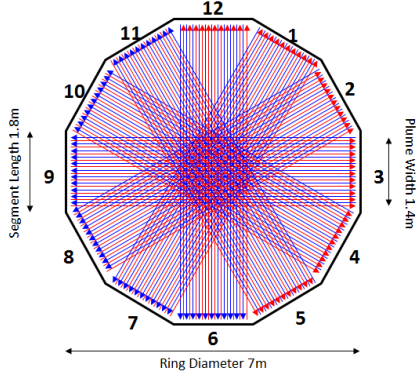


Fig. 7. Optical access beam array as realized for imaging CO₂ at the exhaust of an aviation engine [13]. The array comprises 126 beams arranged in six equi-angular projections each having 21 parallel beams. The engine exhaust plume is contained within a 1.4 m diameter region in the centre of a 1.5 m diameter imaging space.

closely-spaced sampling beams within a projection can be seen in the reconstructions using Tikhonov regularization. The artefacts are particularly pronounced in the 378-beam case (Fig. 8b) where the ratio of projections to beams is 1:10.

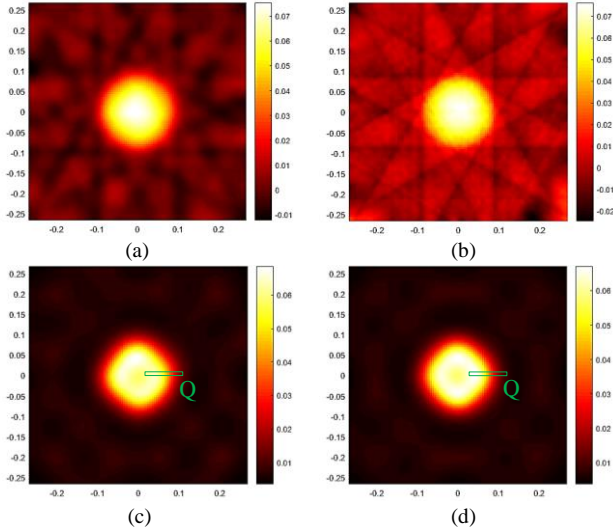


Fig. 8. Tomographic image reconstructions of a simulated, 40 cm diameter sharp-edge circular phantom having a uniform 6% concentration centered in the imaging space formed by the beam geometry shown in Fig. 7. Reconstructions with 126 sampling beams in six projections using Tikhonov regularization (a) and strict positivity (c). Reconstructions under identical conditions but using 378 beams in six projections using Tikhonov regularization (b) and strict positivity (d). The rectangular quantification region Q is shown in (c) and (d).

To quantify the limiting spatial resolution of the system we applied the observer-free method described in [51] based on the decomposition of the spatial frequency content in the reconstructed image. Here, we performed the quantification in a single thin rectangular region (5 by 50 px) centered about the edge of the concentration within the images reconstructed using the positivity constraint for the 126 and 378-beam cases (Fig. 8). The concentration edge within the thin region approximates

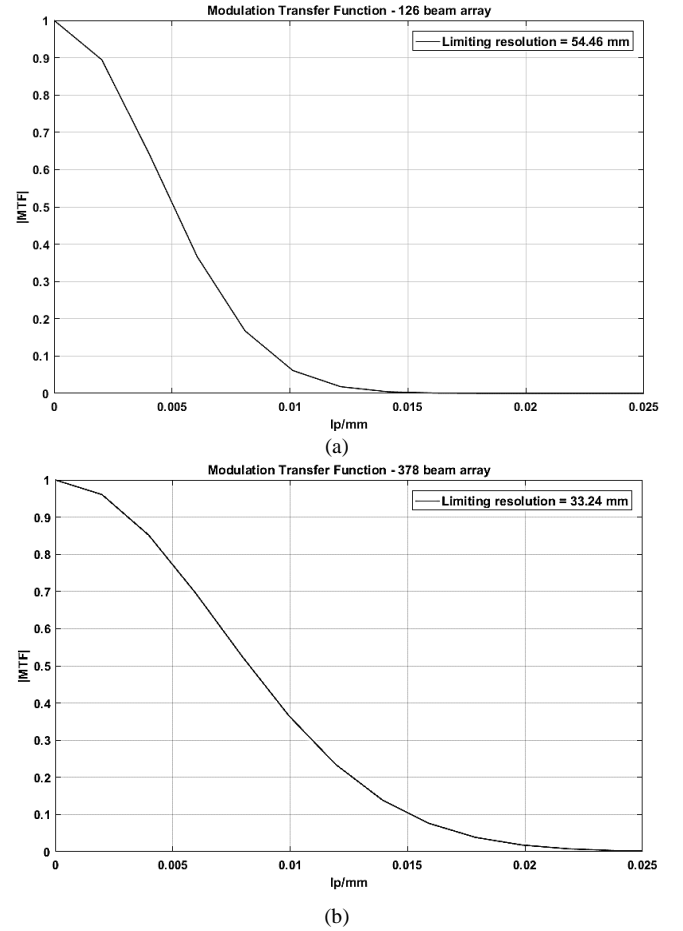


Fig. 9. Modulation Transfer Functions resulting from the spatial resolution quantification regions shown in Fig. 8 for the 126-beam array (a) and 363-beam array (b). The limiting spatial resolution is 54 mm and 33 mm respectively.

a straight edge as described in [51] and we assume that the spatial resolution is uniform within each quantification region.

The quantification algorithm we employed proceeds as follows. The desired image was loaded as a 2D, 8-bit grayscale image. The image was cropped (Matlab `imcrop`) using a thin rectangular window perpendicular to and centered on the edge of interest (regions denoted as ‘Q’ in Fig. 8c and 8d), ensuring that the edge is fully enclosed as described in [51]. The pixel intensity in the cropped strip represents the Edge Spread Function (ESF) at that quantification location. Due to the typically low number of pixels in limited-view reconstructions, the ESF was interpolated by fitting a smoothing spline and then it was oversampled 20 times. The ESF was differentiated (Matlab `diff`) to yield the Line Spread Function (LSF). At this point the LSF remained noisy, so a Gaussian profile was fitted before the LSF being normalised so that the sum of the data values is equal to 1. The Fast Fourier Transform of the LSF was calculated (Matlab `fft`) to yield the Modulation Transfer Function (MTF). Subsequently the absolute value of the MTF was computed and frequency shifted (Matlab `fftshift`), discarding negative spatial frequencies. The spatial frequency axis of the MTF (x-axis) was computed using the Matlab instruction `linspace(-Fs/2, (Fs/2) - (Fs/N), N)`, where F_s is the sampling rate in samples per pixel, and N is the total number of samples (equal to the length of the LSF vector after the

Gaussian fit). At this stage the spatial frequency axis has units of cycles per pixel (equivalent to line pairs per pixel, lp/px) and, in order to convert to line pairs per millimeter (lp/mm), the axis values were divided by the pixel pitch (mm/px). We applied a sharp cut-off point where the absolute value of the MTF is 10% of its maximum (termed MTF10) and read off the corresponding limiting spatial frequency. Finally, the limiting spatial frequency in millimeters was computed using the Rayleigh resolution criterion as described in [51].

The MTF for each quantification region can be seen in Fig. 9. It can be seen that in the case of the 126-beam array the spatial frequency content above 0.01 line-pairs per mm is attenuated to below 0.1, whereas in the 378-beam array case the system can resolve higher spatial frequencies, i.e. ‘transfer’ from input to output without significant attenuation. We computed the limiting spatial resolution at MTF10 to be 54 mm for the 126-beam array and 33 mm for the 378-beam array. This result represents an improvement in spatial resolution of 38%, which we believe is representative for the entire imaging space given the regular array of sampling beams shown in Fig. 7. Nevertheless the quantification process can be repeated in other regions of the image to produce a map of the limiting spatial resolution similar to that in [51]. We also note that except from a more uniform concentration distribution within the phantom, the improvement in spatial resolution is not obvious to the observer of the reconstructed images. Due to there being differences at the intensity of individual pixels, we hypothesize that this is an artefact of the limited dynamic range of the color palette and the monitor.

An important advantage of translated versus fixed optical access is that in the former the sampling beam acts as a ‘bounding beam’ as described in [51] or ‘tangential beam’ as described in [52] and so the boundaries of spatially isolated features can be localized. Moreover, the reconstruction algorithm can utilize this data to introduce super-resolution in the final images. For a fixed beam array to approximate the same effect it would require a high beam density.

VI. CONCLUSIONS

We have presented an overview of optical access schemes as used in optical absorption tomography systems, identifying a lack of technology options to enable a simultaneously high speed and high spatial resolution tomography system. However, recent developments in the field of electro-optic deflectors have achieved performance levels that make them suitable for application in practical optical absorption tomography systems. We evaluated one such electro-optic deflector in the context of tomography and verified that it can achieve a deflection angle of 216 mrad at a speed of 90 kHz, making the unit particularly suitable for imaging of fast processes. We found that using such a deflector to increase the beam density of an existing array, the spatial resolution can improve significantly, by 38%, and the concentration boundaries can be accurately localized. The improvement in spatial resolution is not obvious in the reconstructed images, however the quantification algorithm successfully interprets the intensity differences that exists at a pixel level. Our further work will aim to implement a multi-

deflector system and experimentally verify the improvement in spatial resolution by e.g. reconstructing closely-spaced features.

REFERENCES

- [1] R. K. Hanson, R. M. Spearrin, and C. S. Goldenstein, *Spectroscopy and Optical Diagnostics for Gases*, 1st ed. 2016 edition. Springer, 2015.
- [2] M. Wang, Ed., *Industrial Tomography: Systems and Applications*. Boston, MA: Woodhead Publishing, 2015.
- [3] S. J. Carey, H. McCann, F. P. Hindle, K. B. Ozanyan, D. E. Winterbone, and E. Clough, ‘Chemical species tomography by near infra-red absorption’, *Chem. Eng. J.*, vol. 77, no. 1–2, pp. 111–118, Apr. 2000.
- [4] F. P. Hindle, S. J. Carey, K. Ozanyan, D. E. Winterbone, E. Clough, and H. McCann, ‘Measurement of gaseous hydrocarbon distribution by a near-infrared absorption tomography system’, *J. Electron. Imaging*, vol. 10, no. 3, pp. 593–600, 2001.
- [5] P. Wright *et al.*, ‘High-speed chemical species tomography in a multi-cylinder automotive engine’, *Chem. Eng. J.*, vol. 158, no. 1, pp. 2–10, Mar. 2010.
- [6] N. Terzija, S. Karagiannopoulos, S. Begg, P. Wright, K. Ozanyan, and H. McCann, ‘Tomographic imaging of the liquid and vapour fuel distributions in a single-cylinder direct-injection gasoline engine’, *Int. J. Engine Res.*, vol. 16, no. 4, pp. 565–579, Jun. 2015.
- [7] S.-A. Tsekenis, ‘High speed chemical species tomography for advanced fuels and engines’, The University of Manchester, Manchester, 2013.
- [8] S. A. Tsekenis *et al.*, ‘Towards in-cylinder chemical species tomography on large-bore IC engines with pre-chamber’, *Flow Meas. Instrum.*, 2016.
- [9] L. Ma *et al.*, ‘Tomographic imaging of temperature and chemical species based on hyperspectral absorption spectroscopy’, *Opt. Express*, vol. 17, no. 10, pp. 8602–8613, May 2009.
- [10] F. Wang, Q. Wu, Q. Huang, H. Zhang, J. Yan, and K. Cen, ‘Simultaneous measurement of 2-dimensional H₂O concentration and temperature distribution in premixed methane/air flame using TDLAS-based tomography technology’, *Opt. Commun.*, vol. 346, pp. 53–63, Jul. 2015.
- [11] Y. Deguchi, T. Kamimoto, and Y. Kiyota, ‘Time resolved 2D concentration and temperature measurement using CT tunable laser absorption spectroscopy’, *Flow Meas. Instrum.*, vol. 46, Part B, pp. 312–318, Dec. 2015.
- [12] L. Ma *et al.*, ‘50-kHz-rate 2D imaging of temperature and H₂O concentration at the exhaust plane of a J85 engine using hyperspectral tomography’, *Opt. Express*, vol. 21, no. 1, pp. 1152–1162, Jan. 2013.
- [13] P. Wright *et al.*, ‘Progress towards non-intrusive optical measurement of gas turbine exhaust species distributions’, in *2015 IEEE Aerospace Conference*, 2015, pp. 1–14.
- [14] C. Lindstrom, C.-J. Tam, R. Givens, D. Davis, and S. Williams, ‘Diode laser absorption tomography using data compression techniques’, 2008, vol. 6814, p. 68140W–68140W–17.
- [15] C. J. Dasch, ‘One-dimensional tomography: a comparison of Abel, onion-peeling, and filtered backprojection methods’, *Appl. Opt.*, vol. 31, no. 8, pp. 1146–1152, Mar. 1992.
- [16] R. J. Hall and P. A. Bonczyk, ‘Sooting flame thermometry using emission/absorption tomography’, *Appl. Opt.*, vol. 29, no. 31, pp. 4590–4598, Nov. 1990.
- [17] K. L. McNesby, R. G. Daniel, J. B. Morris, and A. W. Miziolek, ‘Tomographic analysis of CO absorption in a low-pressure flame’, *Appl. Opt.*, vol. 34, no. 18, pp. 3318–3324, Jun. 1995.
- [18] R. Villarreal and P. L. Varghese, ‘Frequency-resolved absorption tomography with tunable diode lasers’, *Appl. Opt.*, vol. 44, no. 31, pp. 6786–6795, Nov. 2005.
- [19] R. J. Santoro, H. G. Semerjian, P. J. Emmerman, and R. Goulard, ‘Optical tomography for flow field diagnostics’, *Int. J. Heat Mass Transf.*, vol. 24, no. 7, pp. 1139–1150, Jul. 1981.
- [20] F.-Y. Zhang, T. Fujiwara, and K. Komurasaki, ‘Diode-laser tomography for arcjet plume reconstruction’, *Appl. Opt.*, vol. 40, no. 6, pp. 957–964, Feb. 2001.
- [21] P. Kauranen, H. M. Hertz, and S. Svanberg, ‘Tomographic imaging of fluid flows by the use of two-tone frequency-modulation spectroscopy’, *Opt. Lett.*, vol. 19, no. 18, pp. 1489–1491, Sep. 1994.

- [22] C. Belotti, F. Cuccoli, L. Facheris, and O. Vaselli, 'An application of tomographic reconstruction of atmospheric CO₂ over a volcanic site based on open-path IR laser measurements', *IEEE Trans. Geosci. Remote Sens.*, vol. 41, no. 11, pp. 2629–2637, Nov. 2003.
- [23] L. Wondraczek, A. Khorsandi, U. Willer, G. Heide, W. Schade, and G. H. Frischat, 'Mid-infrared laser-tomographic imaging of carbon monoxide in laminar flames by difference frequency generation', *Combust. Flame*, vol. 138, no. 1–2, pp. 30–39, Jul. 2004.
- [24] B. Gillet, Y. Hardalupas, C. Kavounides, and A. M. K. P. Taylor, 'Infrared absorption for measurement of hydrocarbon concentration in fuel/air mixtures (MAST-B-LIQUID)', *Appl. Therm. Eng.*, vol. 24, no. 11–12, pp. 1633–1653, Aug. 2004.
- [25] J. A. Silver, D. J. Kane, and P. S. Greenberg, 'Quantitative species measurements in microgravity flames with near-IR diode lasers', *Appl. Opt.*, vol. 34, no. 15, pp. 2787–2801, May 1995.
- [26] C. Liu, L. Xu, J. Chen, Z. Cao, Y. Lin, and W. Cai, 'Development of a fan-beam TDLAS-based tomographic sensor for rapid imaging of temperature and gas concentration', *Opt. Express*, vol. 23, no. 17, pp. 22494–22511, Aug. 2015.
- [27] G. W. Faris and R. L. Byer, 'Quantitative optical tomographic imaging of a supersonic jet', *Opt. Lett.*, vol. 11, no. 7, pp. 413–415, Jul. 1986.
- [28] E. J. Beiting, 'Fiber-optic fan-beam absorption tomography', *Appl. Opt.*, vol. 31, no. 9, pp. 1328–1343, Mar. 1992.
- [29] S. Shimizu and S. Sakai, 'High-Speed Tomography for Simultaneous Measurement of the Histories of Two-Dimensional Distributions of Temperature and Density of Burnt Gases', *JSME Int. J. Ser. B*, vol. 37, no. 3, pp. 596–603, 1994.
- [30] K. Salem, E. Tsotsas, and D. Mewes, 'Tomographic measurement of breakthrough in a packed bed adsorber', *Chem. Eng. Sci.*, vol. 60, no. 2, pp. 517–522, Jan. 2005.
- [31] S. Pal, K. B. Ozanyan, and H. McCann, 'A computational study of tomographic measurement of carbon monoxide at minor concentrations', *Meas. Sci. Technol.*, vol. 19, no. 9, p. 094018, 2008.
- [32] P. Wright *et al.*, 'Toward in-cylinder absorption tomography in a production engine', *Appl. Opt.*, vol. 44, no. 31, pp. 6578–6592, Nov. 2005.
- [33] R. L. Byer and L. A. Shepp, 'Two-dimensional remote air-pollution monitoring via tomography', *Opt. Lett.*, vol. 4, no. 3, p. 75, Mar. 1979.
- [34] K. E. Bennett, G. W. Faris, and R. L. Byer, 'Experimental optical fan beam tomography', *Appl. Opt.*, vol. 23, no. 16, pp. 2678–2685, Aug. 1984.
- [35] F. Wang *et al.*, 'Two-dimensional tomography for gas concentration and temperature distributions based on tunable diode laser absorption spectroscopy', *Meas. Sci. Technol.*, vol. 21, no. 4, p. 045301, 2010.
- [36] W. J. A. Dahm, S.-J. Chen, J. A. Silver, J. A. Mullin, and N. D. Piltch, 'Mixture fraction measurements via WMS-ITAC in a microgravity vortex ring diffusion flame', *Proc. Combust. Inst.*, vol. 29, no. 2, pp. 2519–2526, Jan. 2002.
- [37] K. Busa, E. Bryner, J. McDaniel, C. Goynes, C. Smith, and G. Diskin, 'Demonstration of Capability of Water Flux Measurement in a Scramjet Combustor using Tunable Diode Laser Absorption Tomography and Stereoscopic PIV', in *49th AIAA Aerospace Sciences Meeting including the New Horizons Forum and Aerospace Exposition*, American Institute of Aeronautics and Astronautics, 2011.
- [38] K. Busa *et al.*, 'Measurements on NASA Langley Durable Combustor Rig by TDLAT: Preliminary Results', presented at the 51st AIAA Aerospace Sciences Meeting, Grapevine, TX, United States, 2013.
- [39] C. Yan and Y. Liao, 'Design of a new optical fiber process tomography configuration with high image reconstruction resolution', *Sens. Actuators B Chem.*, vol. 186, pp. 186–192, Sep. 2013.
- [40] V. L. Kasyutich and P. A. Martin, 'Towards a two-dimensional concentration and temperature laser absorption tomography sensor system', *Appl. Phys. B*, vol. 102, no. 1, pp. 149–162, Jul. 2010.
- [41] P. Bechtold, R. Hohenstein, and M. Schmidt, 'Evaluation of disparate laser beam deflection technologies by means of number and rate of resolvable spots', *Opt. Lett.*, vol. 38, no. 16, pp. 2934–2937, Aug. 2013.
- [42] G. R. B. E. Römer and P. Bechtold, 'Electro-optic and Acousto-optic Laser Beam Scanners', *Phys. Procedia*, vol. 56, pp. 29–39, 2014.
- [43] M. Gottlieb, *Electro-Optic and Acousto-Optic Scanning and Deflection*. New York: Marcel Dekker Inc, 1983.
- [44] B. E. A. Saleh and M. C. Teich, *Fundamentals of Photonics*, 2 edition. Hoboken, N.J.: Wiley-Interscience, 2007.
- [45] K. Nakamura, J. Miyazu, Y. Sasaki, T. Imai, M. Sasaura, and K. Fujiura, 'Space-charge-controlled electro-optic effect: Optical beam deflection by electro-optic effect and space-charge-controlled electrical conduction', *J. Appl. Phys.*, vol. 104, no. 1, p. 013105, Jul. 2008.
- [46] K. Nakamura, J. Miyazu, M. Sasaura, and K. Fujiura, 'Wide-angle, low-voltage electro-optic beam deflection based on space-charge-controlled mode of electrical conduction in KTa_{1-x}Nb_xO₃', *Appl. Phys. Lett.*, vol. 89, no. 13, p. 131115, Sep. 2006.
- [47] S. Yagi, 'KTN Crystals Open Up New Possibilities and Applications', *NTT Tech. Rev.*, vol. 7, no. 12, pp. 1–5, 2009.
- [48] S. Yagi and K. Fujiura, 'Electro-optic KTN Devices', *Phys. Procedia*, vol. 56, pp. 40–47, 2014.
- [49] K. Naganuma, J. Miyazu, and S. Yagi, 'High-resolution KTN Optical Beam Scanner', *NTT Tech. Rev.*, vol. 7, no. 12, pp. 1–6, 2009.
- [50] N. Polydorides, S.-A. Tsekenis, H. McCann, V.-D. A. Prat, and P. Wright, 'An efficient approach for limited-data chemical species tomography and its error bounds', *Proc R Soc A*, vol. 472, no. 2187, p. 20150875, Mar. 2016.
- [51] S. A. Tsekenis, N. Tait, and H. McCann, 'Spatially resolved and observer-free experimental quantification of spatial resolution in tomographic images', *Rev. Sci. Instrum.*, vol. 86, no. 3, p. 035104, Mar. 2015.
- [52] P. Kuchment, *The Radon Transform and Medical Imaging*. Philadelphia: Society for Industrial and Applied Mathematics, 2014.



Stylianos - Alexios Tsekenis received the BEng and EngD degrees in electrical and electronic engineering from the University of Manchester, UK in 2009 and 2013 respectively. He received the Pg.Dip degree in Enterprise management from Manchester Business School in 2011. He has held posts at Intel Corporation, Royal Dutch Shell plc. and Blaupunkt GmbH, developing instrumentation systems that are now in world-wide use. He has provided technology and be-spoke design consultancy services to the events and motorsport industries and is the co-founder of an electronic product design company. In 2014, he joined the Agile Tomography Group at the University of Edinburgh, UK as a Research Associate. His current R&D interests are optical tomography systems to image the spatio-temporal distribution of gases. The systems are used to advance automotive, marine and aero engine technologies in order to reduce emissions and optimize energy efficiency.



Nick Polydorides (M'09) received the B.Eng. degree in electrical and electronic engineering from the University of Manchester Institute of Science and Technology, Manchester, U.K., in 1998; the M.Sc. degree in computation from the University of Oxford, Oxford, U.K., in 1999; and the Ph.D. degree in electrical tomography from The University of Manchester, Manchester, in 2002. He held postdoctoral positions with the School of Mathematics, The University of Manchester, and with the Laboratory for Information and Decision Systems, Massachusetts Institute of Technology, Cambridge, MA, USA. In 2010, he was with The Cyprus Institute, Nicosia, Cyprus, as an Assistant Professor. He is currently a Senior Lecturer with the Institute of Digital Communications, School of Engineering, The University of Edinburgh, U.K.